

The small observed scale of AGN–driven outflows, and inside–out disc quenching

Kastytis Zubovas^{1,*} and Andrew King^{2,3,4}

¹Center for Physical Sciences and Technology, Savanorių 231, Vilnius LT-02300, Lithuania

²Department of Physics & Astronomy, University of Leicester, Leicester, LE1 7RH, UK

³Astronomical Institute Anton Pannekoek, University of Amsterdam, Science Park 904, 1098 XH Amsterdam, Netherlands

⁴Leiden Observatory, Leiden University, Niels Bohrweg 2, NL-2333 CA Leiden, Netherlands

* E-mail: kastytis.zubovas@ftmc.lt

26 July 2016

ABSTRACT

Observations of massive outflows with detectable central AGN typically find them within radii $\lesssim 10$ kpc. We show that this apparent size restriction is a natural result of AGN driving if this process injects total energy only of order the gas binding energy to the outflow, and the AGN varies over time (‘flickers’) as suggested in recent work. After the end of all AGN activity the outflow continues to expand to larger radii, powered by the thermal expansion of the remnant shocked AGN wind. We suggest that on average, outflows should be detected further from the nucleus in more massive galaxies. In massive gas-rich galaxies these could be several tens of kpc in radius. We also consider the effect that pressure of such outflows has on a galaxy disc. In moderately gas-rich discs, with gas-to-baryon fraction < 0.2 , the outflow may induce star formation significant enough to be distinguished from quiescent by an apparently different normalisation of the Kennicutt-Schmidt law. The star formation enhancement is probably stronger in the outskirts of galaxy discs, so coasting outflows might be detected by their effects upon the disc even after the driving AGN has shut off. We compare our results to the recent inference of inside–out quenching of star formation in galaxy discs.

Key words: quasars: general — accretion, accretion discs — ISM: evolution — stars: formation — galaxies: evolution

1 INTRODUCTION

Modern galaxy evolution models typically include feedback from active galactic nuclei (AGN) in order to explain the drop-off in the galaxy mass function compared with the expected halo mass function above $M_* \simeq 10^{11} M_\odot$, prevent the cooling catastrophe in galaxy clusters and produce the scaling relations between galaxies and their central supermassive black holes (SMBH). The existence of a feedback link has been all but confirmed observationally, with pc-scale relativistic winds (e.g., Tombesi et al. 010a,b) and massive outflows on scales from sub-kpc (Alatalo et al. 2011) to several kpc (Feruglio et al. 2010; Sturm et al. 2011; Rupke & Veilleux 2011; Ciccone et al. 2014) detected in a number of galaxies, sometimes both types seen in the same object (Tombesi et al. 2015).

Despite this robust general picture, a number of questions remain regarding the effects of AGN feedback upon the host galaxies. One question is the range of spatial scales over which outflows are found. Simple models (e.g., Zubovas & King 2012a) predict outflows propagating with

roughly constant velocity out to very large radii. However, AGN outflows are only detected within the central ~ 10 kpc of the nucleus (e.g., Spence et al. 2016). The fact that AGN outflows should expand for a long time after the driving AGN switches off (e.g., King et al. 2011) might offer an explanation to this problem.

Another question is the possibility of the outflow triggering star formation in the galaxy disc. Such a process has been proposed and investigated before (Silk 2005; Silk & Norman 2009; Gaibler et al. 2012; Zubovas et al. 2013; Silk 2013; Bieri et al. 2016), but there is still no consensus. Observations do not provide a unique answer either, with AGN activity found associated with both elevated (e.g., Santini et al. 2012; Bernhard et al. 2016) and suppressed (e.g., Page et al. 2012; Carniani et al. 2016) star formation in the host galaxy, while sometimes no connection is evident at all (e.g., Bongiorno et al. 2012; Mullaney et al. 2012). One interesting piece of evidence is recent detection of star formation being quenched from the inside out in galaxy discs (Tacchella et al. 2015). We suggest that sim-

ilar behaviour may be expected from disc galaxies affected by AGN outflows.

In this paper, we investigate both the propagation of AGN-driven outflows and their effect on galaxy discs by means of a semi-analytical model. We track the expansion of an outflow driven by a flickering AGN by numerically integrating the equation of motion and find that the outflow is more likely to be detected close to the centre of the galaxy than far away. We assume that the growth of the central black hole and the accompanying AGN activity switches off once the total energy injected into the outflow is of order the binding energy of the gas, because this starves the central black hole. With this assumption we show that outflows are only detectable within ~ 10 kpc of the centre of the host galaxy while the galaxy nucleus is active. Next we use a simple prescription based on the KS law to calculate the expected star formation rate and dynamical pressure in the galactic disc and compare this with the outflow pressure. We find that AGN outflows can produce a significant enhancement of star formation, especially in the outskirts of galaxy discs. This process helps eventually quench star formation from inside out, similar to the suggestion in recent work (Tacchella et al. 2015), by exhausting the available gas supply. It offers a diagnostic tool for detecting remnant outflows which might be unobservable directly.

We structure this paper as follows. In Section 2, we briefly describe the basics of the AGN wind outflow model. In Section 3, we describe the numerical integrator used to follow the evolution of the outflow driven by a flickering AGN and present the results of outflow size. In Section 4, we consider the effect of such an outflow upon the galactic disc and estimate the strength of the starburst. We discuss in Section 5 and conclude in Section 6.

2 WIND OUTFLOW MODEL

To model the AGN feedback we consider the interaction of AGN winds with the surrounding medium, which produces large-scale outflows. This has been presented and investigated in various papers, both analytical (King 2003, 2005, 2010b; Zubovas & King 2012a; Faucher-Giguère & Quataert 2012), and numerical (Nayakshin & Power 2010). Here we briefly summarize the main features. For an extensive summary see King & Pounds (2015).

The central supermassive black hole in a galaxy accretes material from the surroundings via a geometrically thin, optically thick disc. At sufficiently high accretion rates, radiation pressure from the disc and corona drives a wind with mass outflow rate comparable to the accretion rate, i.e. $\dot{M}_w \simeq \dot{M}_{acc}$. The wind is launched with a velocity of order the escape velocity at the launch radius, $v_w \simeq \eta c$, with $\eta \simeq 0.1$ the radiative efficiency of accretion. The wind self-regulates to stay at a Compton optical depth of approximately unity, so that each photon of the AGN radiation field scatters on average once before escaping from the wind. This leads to the wind momentum rate

$$\dot{P}_w = \dot{M}_w v_w \simeq \frac{L_{AGN}}{c} = \dot{P}_{AGN}, \quad (1)$$

and an energy rate

$$\dot{E}_w = \frac{\dot{M}_w v_w^2}{2} \simeq \frac{\eta L_{AGN}}{2}. \quad (2)$$

The wind collides with the interstellar medium (ISM) surrounding the AGN and shocks against it, driving an outflow. The dynamics of the outflow depend on whether the shocked wind cools efficiently. In this paper we are interested in the large-scale outflows that follow the establishing of the $M - \sigma$ relation and sweep the galaxy clear of interstellar gas. In this phase all cooling processes are negligible, so the wind shock is adiabatic. We call this type of outflow energy-driven, because all the AGN wind energy is used to drive the outflow (but note that the forward shock into the ISM need not be adiabatic – in fact there are indications that it may cool strongly; see, e.g., Zubovas & King 2014; Nayakshin & Zubovas 2012). Under ideal circumstances, the AGN wind has a kinetic energy rate $\dot{E}_{out} = \dot{E}_w$ and a momentum rate $\dot{P}_{out} \sim 20\dot{P}_w$ (Zubovas & King 2012a). These winds drive the interstellar gas out of the galaxy bulge at rates of several $100 M_\odot \text{ yr}^{-1}$ and speeds $\sim 1000 \text{ km s}^{-1}$. These results are remarkably consistent with observations of large-scale molecular outflows in galaxies (Rupke & Veilleux 2011; Feruglio et al. 2010; Sturm et al. 2011; Riffel & Storchi-Bergmann 2011b,a; Ciccone et al. 2014), and in one case a driving AGN wind with parameters very close to eqs. (1, 2) is seen simultaneously (Tombesi et al. 2015).

Despite these successes, some parts of this picture need clarification. In particular, most outflows are observed at distances $\lesssim 10$ kpc from the nucleus of the galaxy (e.g., Shih & Rupke 2010; García-Burillo et al. 2015; Spence et al. 2016). The analytical models predict outflow velocities $v_{out} \simeq 1000 \text{ km s}^{-1} \simeq 1 \text{ kpc Myr}^{-1}$ when the AGN is active. Naively, this would mean that observations generally select outflows no more than a few Myr after the start of AGN activity, which is at first sight puzzling. But there is considerable evidence that AGN activity is very time-dependent, with only a short duty cycle (Schawinski et al. 2015; King & Nixon 2015). In the next Section we argue that outflows driven by such ‘flickering’ AGN explain this and other features of the observed outflows.

3 OUTFLOW EXPANSION

3.1 Outflow equation of motion

An energy-driven spherically symmetric outflow expands because of the adiabatic expansion of the wind bubble inside it. The equation of motion for the contact discontinuity between the shocked wind and the shocked ISM can in principle be derived (cf. King 2005; Zubovas & King 2012b) from Newton’s second law and the energy equation. In previous papers we derived this equation of motion for outflows with several simplifying assumptions. Here, we derive it in the most general case which is analytically tractable, keeping only three assumptions:

- the whole system is always spherically symmetric;
- the shocked wind is completely adiabatic;
- the wind bubble moves as a single entity, i.e. there are no significant radial velocity gradients inside the shocked

wind region because the sound crossing time is much shorter than other timescales relevant in the problem.

With these assumptions the motion of the shocked wind bubble is completely specified in terms of the radius $R(t)$ of the contact discontinuity with the ISM. This allows a very simple description at the cost of some loss of detail, since we do not specify the physics of the forward shock, and so exactly how mass is swept up by the expanding wind bubble. Fortunately we will see that our conclusions are not sensitive to the various assumptions one can make here. We consider the effects of making different assumptions in Section 5.1.

In deriving the equation of motion, we specify all vector quantities with respect to the distant upstream medium. We start with the appropriate expression of Newton's second law:

$$\frac{d}{dt} [M\dot{R}] = 4\pi R^2 P - \frac{GM(M_b + M/2)}{R^2}. \quad (3)$$

Here the term on the left hand side is the time derivative of the linear momentum, with $M(R)$ the instantaneous swept-up gas mass being driven out when the bubble (contact discontinuity) is at radius R , P is the expanding gas pressure and M_b is the mass of the stars and dark matter within R (these are left unmoved by the outflow). The factor $1/2$ in the gravity term arises since gas is interacting with itself. This equation gives the gas pressure as

$$P = (4\pi R^2)^{-1} \left[\dot{M}\dot{R} + M\ddot{R} + \frac{GM(M_b + M/2)}{R^2} \right]. \quad (4)$$

Next, we take the energy equation:

$$\frac{d}{dt} \left[\frac{3}{2} PV \right] = \eta L_{\text{AGN}} - P \frac{dV}{dt} - \frac{dE_g}{dt}, \quad (5)$$

where the term on the left hand side is the change in wind internal energy, V is the volume cleared by the outflowing gas and E_g is the gravitational binding energy of the gas. We neglect the kinetic energy of the shocked wind gas since the wind shock is very strong ($v_w \gg \dot{R}$). The gravitational binding energy change is

$$\begin{aligned} \frac{dE_g}{dt} &= -\frac{d}{dt} \left[\frac{GM(M_b + M/2)}{R} \right] \\ &= -G \left[\frac{\dot{M}M_b + M\dot{M}_b + M\dot{M}}{R} - \frac{\dot{R}M(M_b + M/2)}{R^2} \right]. \end{aligned} \quad (6)$$

The first term gives the increase in gravitational binding energy through the increase in outflowing and background mass, while the second gives the decrease in binding energy from the outflow expansion (the binding energy per unit outflowing mass decreases with R , as expected).

The change in internal energy depends to some extent on how the swept-up ISM is added to the outflow. Because the shocked wind gas is extremely dilute, the contact discontinuity is highly Rayleigh–Taylor unstable (King 2005, 2010a) so the shocked ISM is mixed with it rather than forming a thin shell ahead of it. But the fact that the observed outflows show molecular gas moving at speeds $\sim 1000 \text{ km s}^{-1}$ probably also means that the interstellar gas cools very rapidly. By keeping the assumptions of spherical symmetry and outflow uniformity as specified in the begin-

ning of this Section, we find

$$\begin{aligned} \frac{d}{dt} \left[\frac{3}{2} PV \right] &= \frac{d}{dt} [2\pi R^3 P] \\ &= \frac{d}{dt} \left[\frac{\dot{M}R\dot{R} + M\ddot{R}}{2} + \frac{GM(M_b + M/2)}{2R} \right] \\ &= \frac{\ddot{M}R\dot{R} + \dot{M}\dot{R}^2 + \dot{M}R\ddot{R} + \dot{M}\ddot{R} + \dot{M}\ddot{R} + M\ddot{R}\ddot{R}}{2} \\ &\quad + \frac{G}{2} \left[\frac{\dot{M}M_b + M\dot{M}_b + M\dot{M}}{R} - \frac{\dot{R}(MM_b + M^2/2)}{R^2} \right]. \end{aligned} \quad (7)$$

The PdV work term is

$$P \frac{dV}{dt} = 4\pi R^2 P \dot{R} = \dot{M}\dot{R}^2 + M\ddot{R}\dot{R} + \frac{G\dot{R}(MM_b + M^2/2)}{R^2}. \quad (8)$$

Combining the above expressions leads to

$$\begin{aligned} \frac{\eta}{2} L_{\text{AGN}} &= \dot{M}R\ddot{R} + \frac{3}{2}\dot{M}\dot{R}^2 + \frac{3}{2}M\ddot{R}\dot{R} + \frac{1}{2}\ddot{M}R\dot{R} + \frac{1}{2}M\ddot{R}\ddot{R} \\ &\quad - \frac{G}{2} \left[\frac{\dot{M}M_b + M\dot{M}_b + M\dot{M}}{R} + \frac{3\dot{R}(MM_b + M^2/2)}{R^2} \right]. \end{aligned} \quad (9)$$

We rearrange this equation as

$$\begin{aligned} \ddot{R} &= \frac{\eta L_{\text{AGN}}}{MR} - \frac{2\dot{M}\ddot{R}}{M} - \frac{3\dot{M}\dot{R}^2}{MR} - \frac{3\dot{R}\ddot{R}}{R} - \frac{\ddot{M}\dot{R}}{M} \\ &\quad + \frac{G}{R^2} \left[\dot{M} + \dot{M}_b + \dot{M} \frac{M_b}{M} - \frac{3}{2}(2M_b + M) \frac{\dot{R}}{R} \right]. \end{aligned} \quad (10)$$

In all the equations above, $\dot{M} \equiv \dot{R}\partial M/\partial R$ and $\ddot{M} \equiv \ddot{R}\partial M/\partial R + \dot{R}(d/dt)(\partial M/\partial R)$. In the rest of the paper, we refer to the first term on the right hand side of equation (10) as the driving term, the next four terms as the kinetic terms, and the final term (involving the square brackets) as the gravity term.

3.2 Numerical model

We integrate equation (10) numerically to follow the outflow expansion for a specified history of nuclear activity, expressed as a function $L_{\text{AGN}}(t)$. In most cases, when the outflow properties change gradually, the results of the numerical integration do not depend on the chosen integration scheme; we checked that this is so using a third order Taylor integration scheme and both DKD and KDK leapfrog algorithms. These methods produce slight differences in situations where one or more parameters change abruptly and rapidly, but these situations occur only due to the assumed perfect conservation of energy and would not appear in reality, so the choice of the integrator should not introduce errors larger than our other assumptions do. Therefore, the calculations presented below are performed using a third order Taylor integration scheme for outflow radius (and, correspondingly, a second order scheme for velocity and a first order scheme for acceleration). The timestep is adaptive and equal to $\Delta t = f_{\text{CFL}} \min\{R/\dot{R}, \dot{R}/\ddot{R}, \ddot{R}/\ddot{\ddot{R}}\}$, where $f_{\text{CFL}} = 0.1$ is the Courant factor.

The equation of motion has a large number of free parameters specifying the gas and background density distributions and the AGN luminosity, therefore we first an-

alyze the behaviour of a fiducial model and then consider deviations from it. The fiducial model has a galaxy composed of an $M_h = 6 \times 10^{11} M_\odot$ halo which has an NFW (Navarro et al. 1997) density profile with virial radius $r_{\text{vir}} = 200$ kpc and concentration parameter $c = 10$, and an $M = 4 \times 10^{10} M_\odot$ bulge with a Hernquist density profile with scale radius $r_b = 1$ kpc. The gas fraction in the halo is $f_{g,h} = 10^{-3}$, while in the bulge it is $f_{g,b} = 0.8$. The central AGN is powered by accretion on to a black hole of mass $M_{\text{BH}} = 2 \times 10^8 M_\odot$.

We use the same initial conditions for the outflow properties in each simulation, with $R_0 = 0.01$ kpc, $\dot{R}_0 = 400 \text{ km s}^{-1}$ and $\ddot{R}_0 = 0$. In earlier work (King et al. 2011), we showed that the initial conditions have little effect upon the simulation results, provided that the outflow is initially confined to the central parts of the galaxy, as is done here.

We consider a schematic AGN luminosity history describing three stages of SMBH growth. In the first stage, the SMBH grows together with its host galaxy, but generally stays below the mass given by the relevant $M - \sigma$ relation. Some small-scale outflows might be formed during this stage during periods of AGN activity, but these do not have a large-scale impact upon the gas distribution in the galaxy. Accordingly, we do not model this stage. The second stage occurs when episodic AGN activity inflates a large-scale outflow. We model this as a ‘flickering’ AGN, with luminosity equal to L_{Edd} for periods of $t_{\text{on}} = 5 \times 10^4$ yr, separated by some inactive phase, giving an AGN duty cycle f_{AGN} (King et al. 2008; Schawinski et al. 2015; King & Nixon 2015). Using different values of t_{on} has no effect on our overall results. At the end of this stage, the AGN has removed enough gas from its surroundings to completely shut off its own accretion, and so the third stage is marked by a coasting outflow which is not illuminated by an AGN. This history is qualitatively consistent with the cosmological quasar number density function (e.g., Croom et al. 2004; Richards et al. 2006), which shows quasar numbers increasing from high redshifts to $z \simeq 2$ and decreasing after this. In our picture, the increase in quasar numbers happens as SMBHs grow to higher masses, while the decrease occurs once they begin quenching their own gas supplies.

The precise value of AGN energy injection required to quench accretion is difficult to determine. Since the AGN may well be fed by dense gas clumps which are relatively unperturbed by the passage of an energy-driven outflow (Zubovas & King 2014), injection greater than the binding energy of a spherically-symmetric mass distribution may be needed. In addition, the wind has not only to lift the gas against gravity, but also expand itself, doing nonzero PdV work in the process. After some trial and error, we assumed a total luminous energy release of 30 times the gas binding energy in our fiducial model. This gives the wind kinetic energy driving the outflow as $\eta/2 \times 30 = 1.5$ times the gravitational binding energy. For the fiducial model, $E_b = 1.2 \times 10^{59}$ erg, so the AGN has to be active for ~ 4.4 Myr in total, assuming a constant Eddington ratio $l = 1$ during the active phases. We also consider total energy inputs 2 times higher and 2 times smaller than the fiducial one. For each of these, we calculate the expansion of the outflow with AGN duty cycles of 100%, 20%, 10% and 5%.

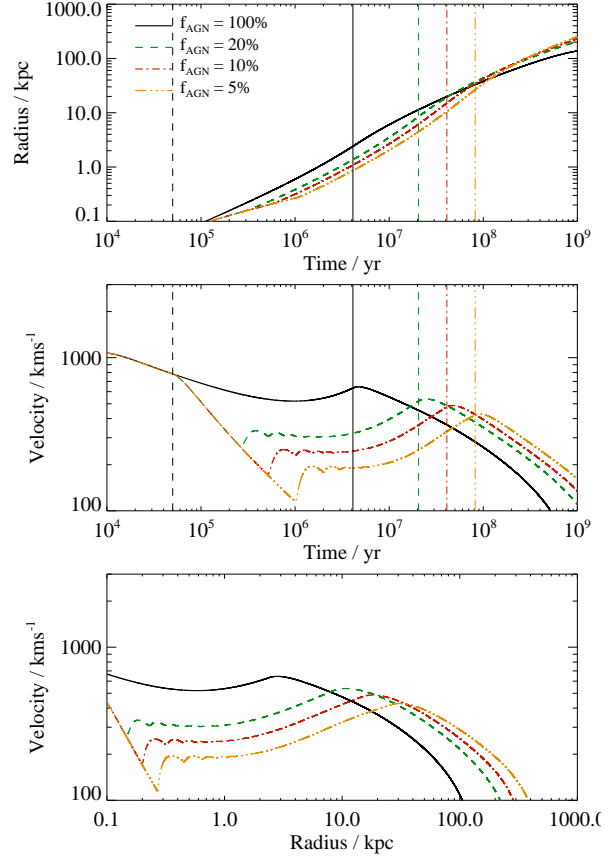


Figure 1. Outflow radius against time (top), velocity against time (middle) and velocity against radius (bottom) plots for the fiducial galaxy parameters (see text) and AGN activity characterised by $t_{\text{on}} = 5 \times 10^4$ yr bursts followed by periods of inactivity giving duty cycles of 100%, 20%, 10% and 5% for black solid, green dashed, red dot-dashed and orange triple-dot-dashed lines, respectively. The thin vertical dashed line indicates the end of the first AGN activity episode and the four thicker vertical lines indicate the final end of AGN activity in the corresponding models. The AGN is switched off completely after releasing an amount of energy equal to $1.5/(\eta/2)$ times the binding energy of the gas.

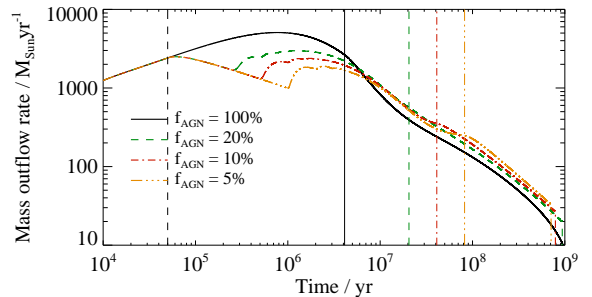


Figure 2. Mass outflow rates for the four models with fiducial galaxy parameters (same as in Figure 1). Colours and line styles are the same as in Figure 1.

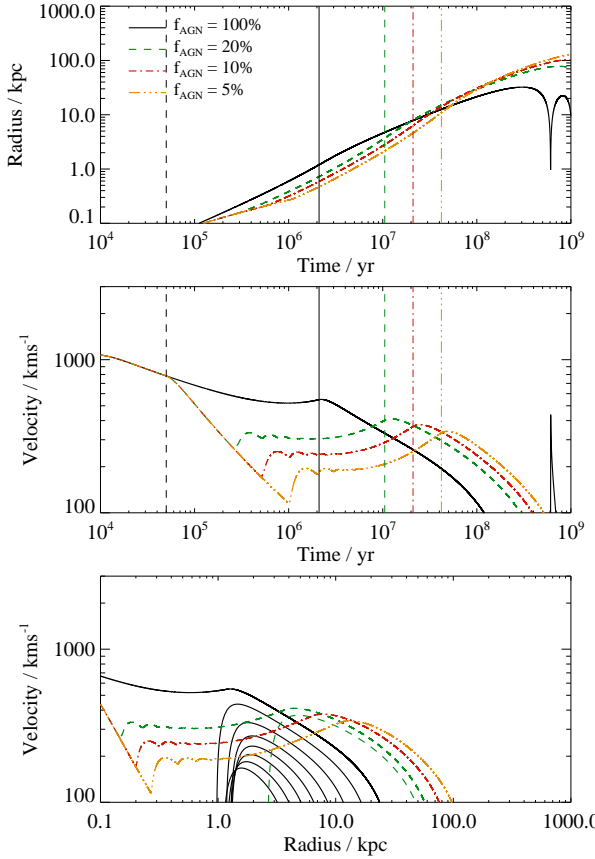


Figure 3. Same as Figure 1, but for total AGN energy injection equal to $0.75/(\eta/2)$ times the binding energy. The outflow stalls and oscillates, leading to the multiple black and green-dashed lines seen in the bottom panel.

3.3 Fiducial model results

In Figure 1, we show the time evolution of the outflow radius (assumed to be given by the contact discontinuity radius $R(t)$; top panel) and velocity $\dot{R}(t)$ (middle panel), and the relation between velocity and radius (bottom panel) for the fiducial model. The vertical dashed line shows the duration of a single AGN activity episode. The AGN shuts off completely at $t = 4.1, 20.5, 41.0$ and 82.0 Myr for the four AGN duty cycles (black solid, green dashed, red dot-dashed and orange dot-double-dashed lines, respectively). Qualitatively, all four outflows expand in a similar fashion. The oscillations caused by AGN flickering smooth out quickly (in < 3 Myr), and the outflow behaves as if driven by an AGN with a lower but constant luminosity. The outflow velocity does not vary significantly with time in any given model and is typically between 200 and 1000 km s^{-1} in all the models considered. These velocities are slightly lower than predicted in our previous work (Zubovas & King 2012a) where we considered outflows in an isothermal potential, and more in line with observed AGN outflows (see Discussion).

Importantly, as shown by King et al. (2011), the outflows continue to expand significantly after the AGN switches off. When the AGN is active, the outflow is within $r = 10$ kpc for 100%, 100%, 72% and 46% of the full cy-

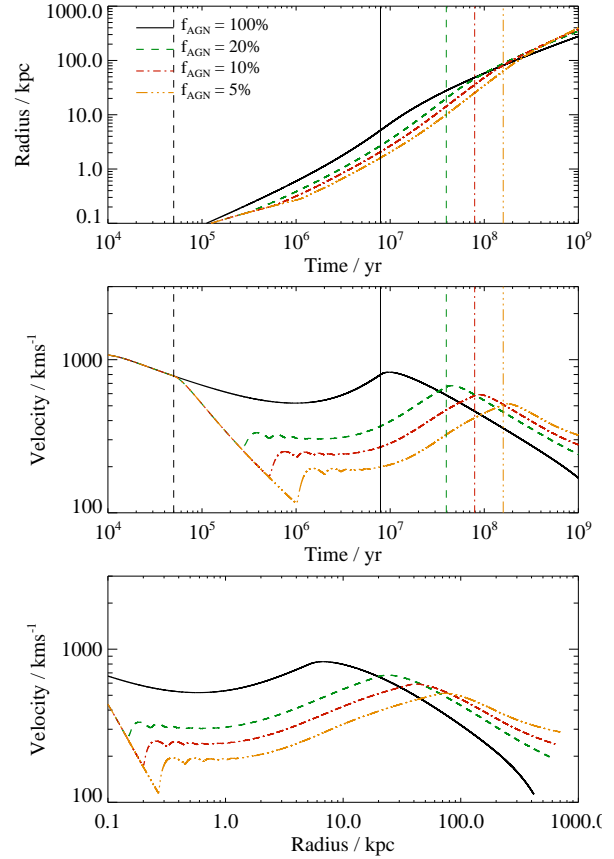


Figure 4. Same as Figure 1, but for total AGN energy injection equal to $3/(\eta/2)$ times the binding energy.

cle, for duty cycles of 100%, 20%, 10% and 5% respectively. We suggest that this may explain the typical spatial extent of manifestly AGN-driven outflows of several kpc (e.g., Shih & Rupke 2010) and the lack of such outflows observed beyond ~ 10 kpc (e.g. Spence et al. 2016). We return to this point in the Discussion.

The mass outflow rate, defined as the time derivative of the baryonic mass contained within R , is also large both while the AGN is active, and for some time after it switches off. The values reached, $\dot{M} > 10^3 M_{\odot} \text{ yr}^{-1}$, should be seen as upper limits, because in reality a significant fraction of the gas is dense and resists being pushed away. Nevertheless, large mass outflow rates need not coincide with AGN activity, therefore the lack of an active nucleus in a given galaxy should not be taken as evidence that any observed outflow is not AGN-driven.

Figures 3 and 4, show the same results as in Figure 1, but for different values of limiting AGN input energy – 0.75 and 3 times the binding energy respectively. We see that if the AGN is very efficient at quenching its own mass supply (Figure 3), the outflows are unable to escape from the halo completely and stall at a few tens to 100 kpc, oscillating afterwards (see the bottom panel). The AGN switches off before any outflow escapes beyond 10 kpc, so we do not expect to see outflows with an active AGN at radii $\gtrsim 10$ kpc. Conversely, a long-lasting AGN episode (Figure 4) clears gas out more easily. The outflow maintains a velocity $\sim 200 \text{ km s}^{-1}$

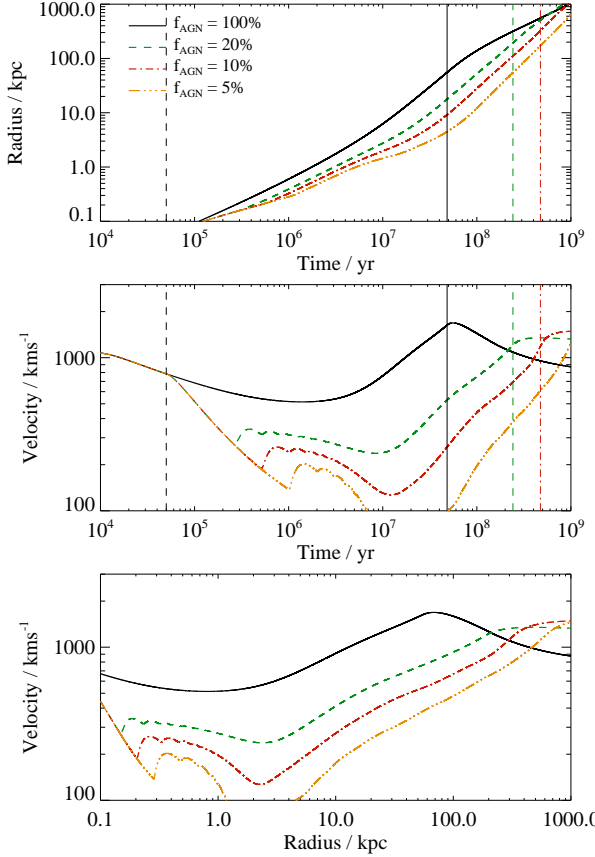


Figure 5. Same as Figure 1, but for a halo with mass $M_h = 10^{13} M_\odot$.

even at $R = 1$ Mpc. In this case, the fraction of outflows within $R = 10$ kpc while the AGN is active is 100%, 57%, 36% and 24% for the four duty cycles. Although some of these outflows do get outside $R = 10$ kpc with the AGN still active, the fractions are still significantly lower than the $\sim 99\%$ expected for an outflow moving at a constant velocity out to $R = 1$ Mpc.

3.4 Trends with halo mass

We also tested how outflows behave in galaxies with different masses. Figures 5 and 6 show the results for galaxies with halo mass $10^{13} M_\odot$ and $10^{11} M_\odot$. We keep the same ratios of $M_{\text{bulge}}/M_{\text{total}}$ and $M_{\text{BH}}/M_{\text{total}}$ as well as gas fractions.

The outflows behave very similarly at early times for all halo masses. This happens because in the central parts of the galaxy (small R) the kinetic terms in the equation of motion (eq. 10) dominate the gravity terms, so the outflow expansion depends mainly on the ratio $L_{\text{AGN}}/M_g \propto M_{\text{BH}}/f_g/M_{\text{total}} = \text{const}$. But the binding energy goes as M^2 , so the time for which the AGN is active is ~ 10 times higher for the $M_h = 10^{13} M_\odot$ halo. In the $M_h = 10^{11} M_\odot$ simulation, we allow the AGN to remain active for long enough to inject 3 times the gravitational binding energy of the gas into the outflow to ensure gas escape, so the activity is ~ 5 times shorter than in the fiducial model.

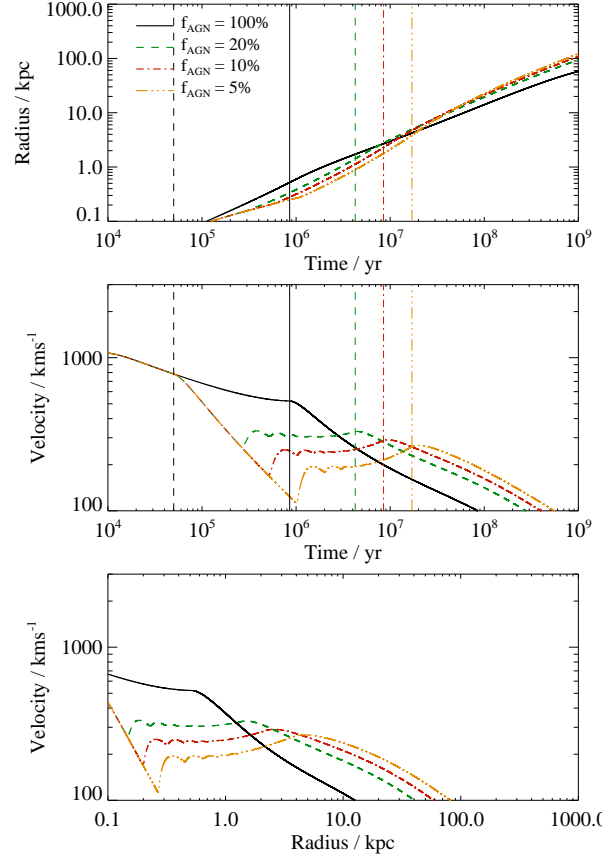


Figure 6. Same as Figure 1, but for a halo with mass $M_h = 10^{11} M_\odot$.

In low-mass halo models, the outflow has only expanded to a few kpc by the time the AGN switches off, and later coasts with a gradually decreasing velocity. Outside ~ 10 kpc the outflow velocity drops below 100 km s^{-1} , making it very difficult to detect.

Conversely, in models with high-mass halos the fraction of outflows within $R < 10$ kpc during phases of AGN activity is 44%, 20%, 16% and 14% for the four AGN duty cycles, respectively. The outflow velocity reaches $\sim 1000 \text{ km s}^{-1}$ before the AGN switches off for the final time, so in this case, outflowing gas would be detectable out to large distances.

4 INDUCED STARBURSTS IN GALAXY DISCS

So far we have discussed the expansion of an outflow driven by a flickering, AGN whose total energy output is limited. We now consider the effects of the outflow pressure on the galaxy disc. We set up a disc extending from 0.125 to 40 kpc in radius, with an exponentially decreasing radial density profile (consistent with observations, e.g., Bigiel & Blitz 2012; Wang et al. 2014), with a scale length of 3 kpc and a total mass $M_d = 3.6 \times 10^{11} M_\odot$. We consider several values of the disc gas fraction $f_{g,d}$: 100%, for a system at high redshift; 50%, for a galaxy which has formed roughly half of its stars (fiducial model); and 20% and 10%, represent-

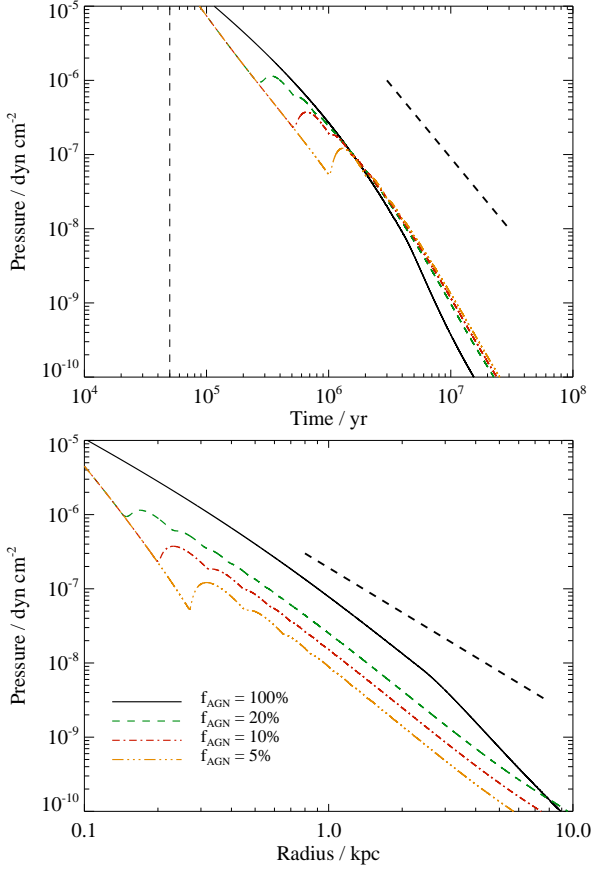


Figure 7. Outflow forward shock pressure against time (top) and radius (bottom). Lines indicate models with AGN duty cycles of 100% (black solid), 20% (green dashed), 10% (red dot-dashed) and 5% (yellow triple-dot-dashed). The AGN is switched off completely after releasing $1.5/(\eta/2)$ times the binding energy of the gas. Thick dashed lines show $p \propto t^{-2}$ and $p \propto R^{-2}$ dependencies.

ing galaxies in the Local Universe. We calculate the star formation rate based on the volumetric Kennicutt–Schmidt relation:

$$\rho_{\text{SFR}} = \epsilon_* \frac{\rho_g}{t_{\text{ff}}} = \epsilon_* \left(\frac{32G}{3\pi} \right)^{1/2} \rho_g^{3/2}, \quad (11)$$

which can be recast for simplicity into a relation based on surface densities:

$$\begin{aligned} \Sigma_{\text{SFR,sp}} &= \epsilon_* \left(\frac{32G}{3\pi} \right)^{1/2} \Sigma_g^{3/2} h_d^{-1/2} \\ &\simeq 4.5 \times 10^{-3} \Sigma_{10}^{3/2} h_{300}^{-1/2} \epsilon_{0.02} \text{M}_{\odot} \text{yr}^{-1} \text{kpc}^{-2}, \end{aligned} \quad (12)$$

where $\epsilon \equiv 0.02\epsilon_{0.02}$ is the star formation efficiency per dynamical time, ρ_g is the gas volume density, $\Sigma_g \equiv 10\Sigma_{10}\text{M}_{\odot}\text{pc}^{-2}$ is the gas surface density and $h_d \equiv 300h_{300}\text{pc}$ is the scale height of the disc. We choose a value for the scale height which gives the appropriate scaling for the Kennicutt–Schmidt relation (Kennicutt 1998).

External compression caused by the passing outflow can stimulate star formation in the disc by reducing the effective dynamical time of star-forming clouds (Zubovas et al. 2014).

We parameterize this as

$$\Sigma_{\text{SFR,ind}} = \Sigma_{\text{SFR,sp}} \left[\left(1 + \frac{P_{\text{ext}}}{P_d} \right)^{\beta} - 1 \right], \quad (13)$$

where

$$P_d = \rho_g c_s^2 = \Sigma_g h_d \left(\frac{v_{\phi}(r)}{r} \right)^2 \quad (14)$$

is the disc pressure at radius r , and β is a free parameter of the model. P_{ext} is the external pressure acting upon the disc (see below), which may be higher or lower than the disc pressure, but would act as an additional compressive term either way. In the simplest case, where external pressure is added linearly to the gravitational energy density, $\beta = 1$, but effects such as pressure instabilities following passage of a shock wave (Hopkins & Elvis 2010) and/or the formation of instabilities behind the shockwave (Zubovas et al. 2014) may decrease ($\beta < 1$) or increase ($\beta > 1$) the SFR enhancement respectively.

To calculate the external pressure we consider the outflow to be composed of two regions: inside the contact discontinuity, the pressure is constant and equal to P_{cd} , while outside the discontinuity it changes linearly between P_{cd} and P_{out} , where the two pressures are calculated as in (cf. Zubovas et al. 2013, and equation 4):

$$P_{\text{cd}} = \frac{1}{4\pi R^2} \left[\frac{d}{dt} [M\dot{R}] + \frac{GM(M_b + M/2)}{R^2} \right], \quad (15)$$

$$P_{\text{out}} = \frac{4}{3} \rho_{\text{amb}} \dot{R}^2. \quad (16)$$

Here the masses include only material within R , and ρ_{amb} is the density of the ambient medium at radius R . In writing the expression of P_{out} , we make an assumption that the radius of the outer shock is $4/3$ times the radius of the contact discontinuity. This is a reasonable assumption so long as the velocity of the outflow is significantly higher than the sound speed in the gas (cf. Zubovas & King 2012a). We plot the evolution of P_{out} with time and radius in the top and bottom panels of Figure 7, respectively. It is worth noting that the radiation pressure $p_{\text{rad}} = L/(4\pi R^2 c)$ is ~ 15 times lower than P_{out} even when $L = L_{\text{Edd}}$, i.e. the outflow has a considerably higher pressure than the radiation field driving it.

4.1 Fiducial model results

We give first the results of the fiducial model (disc gas fraction 50%) with four AGN duty cycles, as above. Figure 8 shows the rates of induced star formation (thick lines) as functions of time. The thin lines represent the ‘spontaneous’ star formation rate $\dot{M}_{\text{SFR,sp}}$, i.e. that given by integrating the KS law (eq. 12) over the whole disc; this SFR decreases with time as gas is consumed in the disc. In the model with continuous AGN activity (black solid line), induced star formation keeps growing until the AGN switches off at $t \simeq 4.1\text{ Myr}$, but never reaches the level of spontaneous star formation, falling short by about a factor of 2. The situation is similar for the lower AGN duty cycles, except that there the induced SFR fluctuates significantly between the ‘on’ and ‘off’ phases of the AGN. This suggests that AGN-induced star formation would be difficult to detect in an

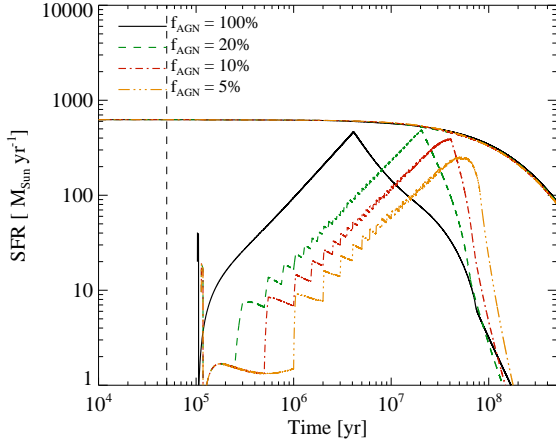


Figure 8. Star formation rate versus time for the models with varying AGN duty cycles: 100% (black solid), 20% (green dashed), 10% (red dot-dashed) and 5% (yellow triple-dot-dashed). The gas fraction in the disc is 50% and the total disc mass is $3.6 \times 10^{11} M_{\odot}$. The AGN is switched off completely after releasing $1.5/(\eta/2)$ times the binding energy of the gas. Thin lines represent spontaneous star formation in the corresponding models.

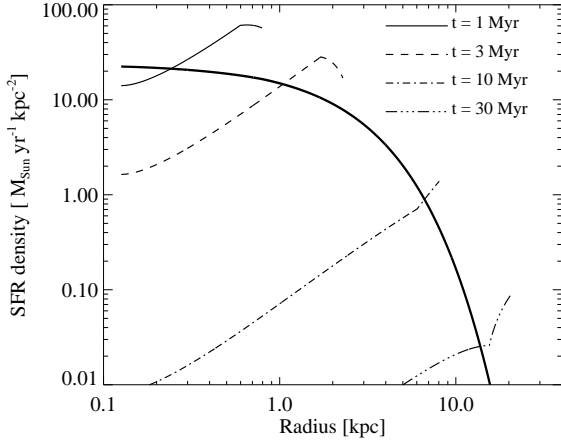


Figure 9. SFR density as function of radius in the fiducial model with 100% AGN duty cycle. Solid line: $t = 1$ Myr after the AGN switches on; dashed line: $t = 3$ Myr; dot-dashed line: $t = 10$ Myr; triple-dot-dashed line: $t = 100$ Myr. Thick solid line shows the spontaneous SFR density profile at $t = 1$ Myr; this profile remains qualitatively similar, but globally decreases, at later times.

unresolved galaxy where only the integrated SFR could be estimated.

If the galaxy disc can be resolved, AGN effects upon star formation are more easily detected. Figure 9 shows the radial SFR density profiles of spontaneous (thick solid line) and induced (thin lines) star formation at different times from 1 to 30 Myr. As expected, the induced SFR at a given radius decreases with time as the outflow expands and the pressures at the centre and the contact discontinuity drop. The induced SFR increases with radius out to the contact discontinuity at all times. This happens because even though the outflow pressure is uniform inside the contact discontinuity, the internal disc pressure decreases with decreasing Σ_g and radius, so the outflow pressure becomes more sig-

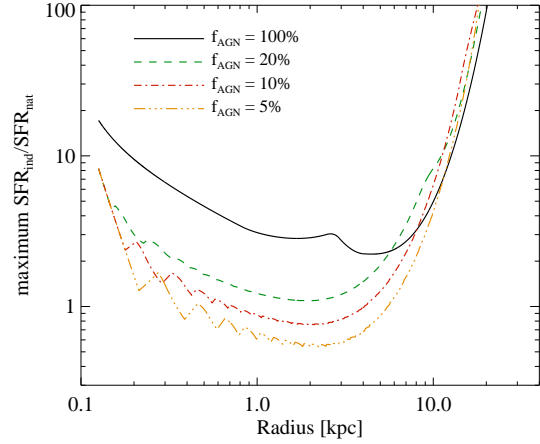


Figure 10. Maximum ratio of induced to spontaneous SFR density as function of radius in the fiducial models. Line styles and colours as in Figure 8.

nificant. The outflow-to-disc pressure ratio increases from typically negligible values close to the centre to $P_{\text{ext}}/P_d \sim 3$ at the outer edge of the outflow. Conversely, as long as the AGN is active, the pressure at the outer shock decays with time more slowly than the pressure at the contact discontinuity because of the increase in outflow velocity, so the ratio of induced SFR density at the outermost point in the disc affected by the outflow to the induced SFR density at the contact discontinuity increases with time. Together, these effects lead to a situation where the star formation enhancement is more significant in the outskirts of the disc than the centre.

We show this result in Figure 10, where we plot the maximum ratio of the value $\Sigma_{\text{SFR,ind}}/\Sigma_{\text{SFR,nat}}$ at every radius in the disc attained before the AGN finally switches off. In the central kiloparsec, this ratio decreases with increasing radius and is only of order a few, but beyond $r \simeq 2 - 6$ kpc, depending on f_{AGN} , it starts growing and reaches a value > 100 at ~ 20 kpc, growing slightly faster with decreasing AGN duty cycle. The fiducial models reveal that AGN outflows can significantly increase the galactic disc SFR within the central kiloparsec and outside ~ 10 kpc, but the effect on integrated SFR parameters is only moderate.

4.2 Star formation triggering in discs with different gas content

We next consider the effects of an AGN outflow upon galaxy discs with different gas fractions. We present results only for a model with $f_{\text{AGN}} = 20\%$, as we believe this to be the most likely of the four AGN duty cycles we investigate (see Section 5.1, below), and models with other values of f_{AGN} show qualitatively similar behaviour (see Figure 8). The expected trend with changing gas density is that the spontaneous SFR decreases as $\Sigma_g^{3/2}$, while the induced SFR decreases only as $\Sigma_{\text{SFR,nat}}/P_d \propto \Sigma_g^{1/2}$. The ratio of the two increases with decreasing gas fraction as $\Sigma_g \propto f_{g,d}$.

Figure 11 shows the star formation histories of models with four different gas fractions. As before, thin lines are spontaneous star formation, while thick ones show induced SFR. As expected, the spontaneous star formation

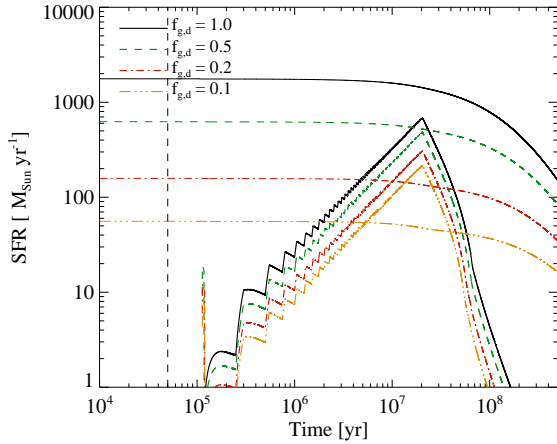


Figure 11. Star formation rate versus time for the models with varying disc gas fractions: 100% (black solid), 50% (green dashed), 20% (red dot-dashed) and 10% (yellow triple-dot-dashed). The AGN is switched off completely after releasing $1.5/(\eta/2)$ times the binding energy of the gas. Thin lines represent spontaneous star formation in the corresponding models.

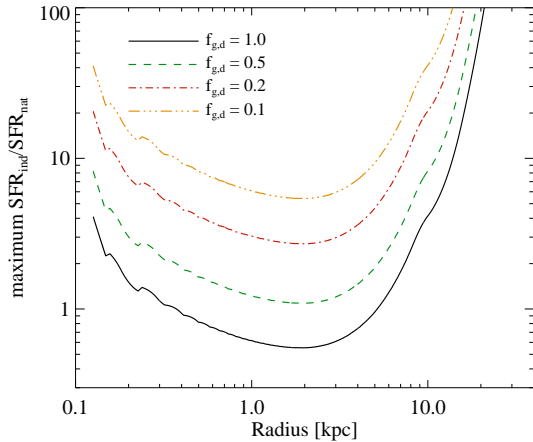


Figure 12. Maximum ratio of induced to spontaneous SFR density as function of radius in the models with varying disc gas fraction. Line styles and colours as in Figure 11.

rate declines as $f_{g,d}^{1.5}$. The induced star formation rate declines slightly faster than $f_{g,d}^{0.5}$, mainly because gas is completely consumed in some annuli of the disc in the lower density simulations, further reducing the integrated SFR. For gas fractions 0.2 and 0.1, corresponding to initial disc gas masses of 7.2 and $3.6 \times 10^{10} M_{\odot}$, the induced SFR is higher than the spontaneous SFR for several Myr. Importantly, the SFR enhancement persists after the AGN switches off, as the outflow is still moving through the galaxy. So in gas-poor galaxy discs AGN activity may induce starbursts which might be visible even in integrated SFR data as offsets from the KS relation.

The ratio of induced to spontaneous SFR is presented in Figure 12. The expected trend is visible there as well, with induced starbursts in low-density galaxy discs increasing the star formation efficiency by more than an order of magnitude from the centre to the outskirts. All four models show qualitatively identical behaviour. The ratio decreases

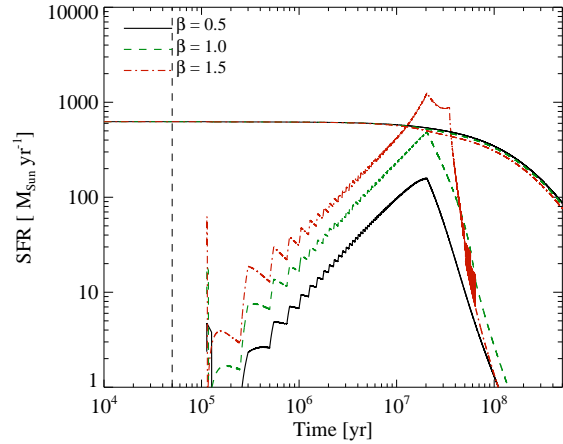


Figure 13. Star formation rate versus time for the models with 50% disc gas fraction and varying star formation induction parameter β : $\beta = 0.5$ (black solid), $\beta = 1$ (green dashed) and $\beta = 1.5$ (red dot-dashed). The AGN is switched off completely after releasing $1.5/(\eta/2)$ times the binding energy of the gas. Thin lines represent spontaneous star formation in the corresponding models.

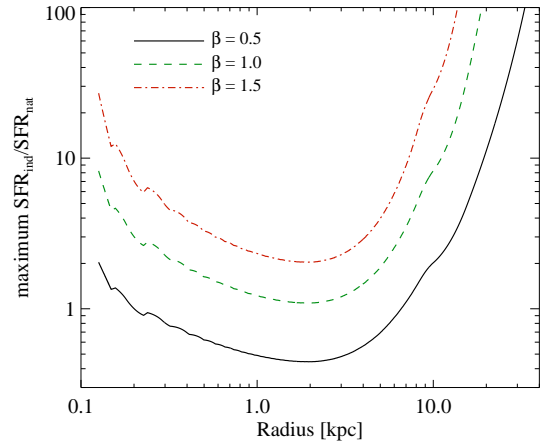


Figure 14. Maximum ratio of induced to spontaneous SFR density as function of radius in the models with varying β . Line styles and colours as in Figure 13.

out to ~ 5 kpc and then increases further out. The bump at $R \simeq 2.5$ kpc appears because the AGN switches off when the outflow has expanded to that distance, and so the outflow pressure begins to drop rapidly.

4.3 Alternative prescriptions for induced star formation

Given that the precise effect of the outflow compression upon the ISM is uncertain, we test four different power-law indices β for the calculation of the induced SFR (eq. 13). The results for $\beta = 0.5, 1$ and 1.5 are shown in Figure 13. As expected, the induced SFR is higher for higher values of β . If $\beta = 0.5$, i.e. the disc resists compression via processes other than star formation feedback, the induced SFR is $\sim 2-3$ times lower than in the fiducial model. On the other hand, $\beta = 1.5$ produces induced SFR becoming higher than the

spontaneous SFR at the peak at $t \simeq 4$ Myr. This induced SFR value is a factor ~ 2 higher than in the fiducial model for the first ~ 10 Myr. Later, as the outflow expands to the disc outskirts, SFR induction is so efficient that the total induced SFR begins to rise with time. The second peak at $t \sim 40$ Myr represents the time when gas is completely consumed in some disc annuli around $R = 20 - 22$ kpc. As star formation stops there, the total induced SFR drops significantly as well.

The radial induced starburst plot (Figure 14) shows the same qualitative behaviour for all three models, with the weakest starburst induced just outside the bulge ($R = 2 - 7$ kpc) and increasing both inward and outward. Even a reduced-efficiency ($\beta = 0.5$) SFR induction can result in a noticeable starburst at $r > 20$ kpc – the derived star formation efficiency is an order of magnitude greater than predicted by the KS law. The extreme ratios achieved for the enhanced-efficiency ($\beta = 1.5$) induction model provoke rapid consumption of gas in the outskirts of the disc, and such powerful starbursts may be difficult to detect because of their short lifetimes.

5 DISCUSSION

5.1 What is the likely duty cycle of AGN? Outflow detectability

By considering the fraction of AGN host galaxies which have not yet been ionised by the X-rays and UV from the nucleus, Schawinski et al. (2015) infer that AGN phases typically last only $\sim 10^5$ yr. A similar result is reached by considering the time required to accrete a disc with outer edge (and hence mass) bounded by self-gravity (King & Nixon 2015). In our model, a single short phase like this is certainly not enough to inflate a massive outflow, so multiple phases of AGN activity are required. Our results depend on the fraction of time that the AGN is active, and we consider simple arguments constraining the possible values of this fraction.

Given the observed fraction of galaxies which are active (e.g., Xue et al. 2010) we should have $f_{\text{AGN}} \sim 5\%$ averaged over the age of the galaxy. A similar fraction comes from the Soltan argument (Soltan 1982). If an SMBH grows from stellar $M_{\text{init}} \sim 10M_{\odot}$ to its present mass, it must spend at least $\ln(M_{\text{fin}}/M_{\text{init}}) \sim 16$ Salpeter times accreting material. This duration is $16t_{\text{Sal}} \sim 670 \text{ Myr} \sim 0.05t_{\text{H}}$, where t_{H} is the Hubble time. However, as the galaxy evolves, the frequency of AGN activity evolves as well. At high redshift there is a lot of gas available to feed the SMBH and the galaxy may be active more often, while at low redshift it is hardly ever active. The phase of gas ejection via a massive outflow marks the end of the high-activity phase of galaxy evolution, and so should be marked by a typical f_{AGN} larger than the long-term average. So our simulations with $f_{\text{AGN}} = 5\%$ represent a lower limit to the expected AGN fraction at this stage of galaxy evolution. We expect $f_{\text{AGN}} \sim 10\%, 20\%$ to be more representative of reality, but the actual value is uncertain.

Our results then suggest that massive outflows are typically detected close to AGN because AGN switch off for good by the time outflows move far out from the nucleus. Outflow signatures might be detectable around inactive galaxies at higher distances than around active galaxies, however as the

outflow expands without driving, its density and velocity decrease and it becomes progressively more difficult to detect. Outflows might also be detectable further from the AGN in more massive galaxies than in lower-mass ones, where the AGN needs to be active for longer and drive the outflow further away to ensure quenching of the mass supply.

Another interesting consequence of having $f_{\text{AGN}} < 1$ is that even in the central parts of galaxies, AGN-driven outflows might often be detected without the presence of the driving AGN itself. These outflows might be erroneously identified as driven by star-formation activity. Therefore, we predict that a larger fraction of outflows happen due to AGN activity than expected from a naive interpretation of observations.

It is important to consider how these results depend on the assumptions we made regarding the model. Real outflows are not uniform nor spherically symmetric, therefore there is a spread of radii at which the outflow is observed at any given time. The spread is mediated by Rayleigh-Taylor instabilities (King 2010a) and by the presence of dense material in the undisturbed ISM, thus the outflowing gas should be seen both closer to the AGN and further away from it than the formal radius of the contact discontinuity. The dense molecular gas, which is the usual tracer of these outflows, is more likely to lag behind the contact discontinuity than ahead of it (see, e.g., the numerical simulations by Nayakshin & Zubovas 2012), therefore our conclusion that outflows should be detected close to their parent AGN is only strengthened.

Another issue is the total energy input by the AGN required to shut off its own accretion. In principle, the dense gas in the galaxy might not be removed even if the outflow clears the diffuse gas, and thus AGN might still be fed by infalling clouds. However, several processes might prevent long-term feeding of an AGN after a large-scale outflow is driven away:

- The fraction of dense gas in galaxy bulges is not very large to begin with, $M_{\text{dense}}/M_{\text{gas}} \lesssim 0.5$ (Blanton & Moustakas 2009; Saintonge et al. 2011; Popping et al. 2014). Therefore, the outflow removes more than half of the material that might eventually feed the AGN.
- The outflow moves past molecular clouds and either disperses them (Hopkins & Elvis 2010) or compresses them and enhances star formation (Zubovas et al. 2014), further depleting the amount of dense gas available to feed the AGN.
- Once the diffuse gas is gone, molecular gas is not replenished any more.

Taken together, these points suggest that most of the AGN feeding reservoir is depleted, or at least significantly diminished, by the large-scale outflow. In addition, our choice for basing the total AGN energy release on the binding energy of the gas is consistent with numerical hydrodynamical simulations which suggest that dark matter halo masses, and hence the binding energies of those haloes, are the most important parameter setting the mass of the SMBH (Booth & Schaye 2010). Therefore we are confident in suggesting that once the AGN outflow unbinds most of the gas from the galaxy, the AGN switches off, essentially, forever.

5.2 Induced starbursts in nuclear gas rings

Starbursts induced by the AGN outflow are stronger in the central kiloparsec compared with the intermediate regions (Figures 10, 12 and 14). This happens because the outflow pressure is very high there, while the disc gas density, and hence its pressure, does not vary strongly within the central scale length.

These sub-kpc scales fall within the bulge of the galaxy, and correspond to locations of nuclear gas and stellar rings seen in many barred galaxies (e.g., Kormendy & Kennicutt 2004; Knapen 2005; Böker et al. 2008). Gas in the rings may be directly affected by the radial push of the AGN wind (Zubovas 2015), but could also be compressed vertically and produce strong bursts of star formation, as observed (Allard et al. 2006; Sarzi et al. 2007). However, any such burst would probably be short, lasting for only a few Myr before the nuclear ring relaxes to a baseline state, and so is probably detectable only simultaneously with AGN activity or soon after the AGN has switched off. Bulge stars and gas may also mask the effect of the outflow on the nuclear gas ring, hampering simple interpretation of the observations.

5.3 Starbursts on galactic outskirts

In the outskirts of galaxy discs, gas density is low, resulting in low pressure and low spontaneous star formation rate density. Therefore, even though the induced star formation rate density decreases as well (see Figure 9), the ratio between the two grows once the outflow moves beyond ~ 5 kpc (see Figure 10). Outside $R \simeq 10$ kpc, this ratio is more than an order of magnitude. Such an offset from the typical values predicted by the KS law should be easily detected, provided that star formation in the galaxy is spatially resolved. Some examples of such galaxies might be the ring galaxies such as the Cartwheel. Detection of rings of star formation with very high star formation efficiency in galactic outskirts might be taken as evidence of recent (less than a few times 10^7 yr) episode of nuclear activity in the galaxy, especially since the star formation efficiency generally tends to decrease in galactic outskirts (Leroy et al. 2008).

5.4 Inside-out quenching of star formation in galaxy discs

Recently, Tacchella et al. (2015) found evidence that star formation in galaxy discs might be quenched from the inside out. This quenching might simply be the result of faster gas depletion in the central parts of the galaxy due to differences in dynamical time. On the other hand, starbursts induced by AGN outflows might enhance this effect.

The induced star formation rate depends strongly on the outflow pressure, which, in turn, depends on its velocity (see Figure 7). As a result, when the outflow is driven by a flickering AGN, induced star formation rate rises periodically during the active phases, and decays during the inactive phases, even though the outflow itself keeps expanding (see Figures 8, 11 and 13). During each active phase, the outflow encompasses a greater part of the disc and leads to faster consumption of gas there. If the gas fraction in the disc is already low, the induced star formation might consume gas and quench star formation in the disc from the

inside out. This process would manifest itself afterward by a radial gradient of stellar ages, however, since the outflow expands at a few hundred km/s, i.e. covers 1 kpc in a few Myr, the gradient might be too shallow to detect easily.

5.5 Flaring of discs in response to outflow passage

One more effect that the outflow might have upon a galaxy gas disc is causing it to flare in response to the outflow passage. This can be seen by considering the following simple argument.

The pressure wave induced by the passing outflow moves vertically through the disc with a velocity

$$v_{\text{sh}} \sim \sqrt{\frac{P_{\text{ext}}}{P_{\text{d}}}} c_{\text{s}}, \quad (17)$$

and takes a time

$$t_{\text{sh}} \sim \frac{2H}{v_{\text{sh}}} \sim 2\sqrt{\frac{P_{\text{d}}}{P_{\text{ext}}}} t_{\text{dyn}} \quad (18)$$

to reflect back to the edge of the disc. In this time, the edge of the outflow has moved outward a distance

$$\Delta R_{\text{out}} \sim v_{\text{out}} t_{\text{sh}} \sim 2 \frac{v_{\text{out}}}{\sigma} \sqrt{\frac{P_{\text{d}}}{P_{\text{ext}}}} \sigma t_{\text{dyn}} \sim 2 \frac{v_{\text{out}}}{\sigma} \sqrt{\frac{P_{\text{d}}}{P_{\text{ext}}}} R, \quad (19)$$

where R is the original outflow location. Putting in typical values $v_{\text{out}}/\sigma \sim 5$, $P_{\text{ext}}/P_{\text{d}} \sim 100$, we find that $\Delta R \sim R$, i.e. the outflow expands to twice the initial radius by the time the induced shockwave reflects back to the edge of the disc. At the edge, the shockwave now encounters outflow pressure which is a factor ~ 4 lower than the pressure which drove the shockwave. Assuming that the shockwave did not lose a significant fraction of its energy (and pressure) during its vertical passage through the disc, it causes the disc to expand until the pressure approximately equilibrates. The expansion factor in disc thickness is comparable to the pressure ratio, i.e. $H'/H \sim 4$. Given that the external pressure becomes progressively more dominant over disc internal pressure as the outflow expands (see Fig. 10 and Section 5.3), disc expansion should be more prominent in the outer parts of the disc, leading to flaring qualitatively consistent with observations (van der Kruit 1981; Momany et al. 2006; Merrett et al. 2006; Vollmer et al. 2016).

5.6 Comparison with other work

In recent years, several authors investigated AGN-triggered star formation in galaxy discs. Silk (2013) provides estimates of the star formation rate enhancement due to increased pressure, with general results very similar to ours. The conclusions of that paper state that quasar-mode feedback should be able to produce such increased pressures, although the focus of the paper was on jet-induced pressure increase. We show that high pressures, similar to the fiducial values assumed by Silk (2013), are a plausible result of AGN wind-driven outflows.

Numerical simulations have so far considered mainly compression of galaxy discs by AGN jet-inflated bubbles (Gaibler et al. 2012; Bieri et al. 2016). Although these simulations consider significantly different physical processes from ours, the general results are qualitatively similar. In

particular, Gaibler et al. (2012) found that a jet-driven outflow in a clumpy medium produces a bubble which expands and compresses a turbulent galaxy disc, leading to enhancement of the star formation rate by a factor of a few from the baseline undisturbed disc SFR. Bieri et al. (2016) found a stronger SFR enhancement, but investigated a longer-duration evolution of a model system, in which a jet-driven cocoon cools down and falls back on to the galaxy disc. Our results, therefore, provide a somewhat different mechanism for inducing higher rates of star formation in a galaxy disc, one which operates on timescales of 1-100 Myr. However, more detailed simulations are required in order to distinguish the predictions of this model from those mentioned above.

6 SUMMARY AND CONCLUSION

We have used a largely analytic model to follow the evolution of a spherically-symmetric, energy-driven AGN outflow expanding in a realistic galaxy environment with an NFW halo and a Hernquist bulge. We showed that if the nucleus remains active only long enough to inject enough energy into the gas to unbind it, then the outflow can only be detected simultaneously with the AGN when its radius is $\lesssim 10$ kpc, consistent with observations. Outflows detected at greater distances in inactive galaxies may point to recent episodes of nuclear activity which have already ended. We also predict that outflows in more massive active galaxies will typically be detected at larger distances from the nucleus than those in lower-mass galaxies.

We have shown that the outflow pressure can enhance star formation in a galaxy disc, producing observable differences in the normalisation of the KS law for the host, at least if the disc is not extremely gas-rich. The SFR enhancement is strongest in the centre and the outskirts of the disc (< 1 kpc and > 10 kpc from the centre, respectively), so these regions are the best places to look for the effects of recent AGN activity. In particular, enhanced star formation efficiency in the outskirts of a galaxy's disc can be used as another diagnostic of an AGN phase within the last few times 10^7 yr.

ACKNOWLEDGMENTS

KZ is funded by the Research Council Lithuania through the National Science Programme grant no. LAT-09/2016. Astrophysics research at the University of Leicester is funded by an STFC Consolidated grant.

REFERENCES

- Alatalo K., Blitz L., Young L. M., Davis T. A., Bureau M., Lopez L. A., Cappellari M., Scott N., et al. 2011, *ApJ*, 735, 88
- Allard E. L., Knapen J. H., Peletier R. F., Sarzi M., 2006, *MNRAS*, 371, 1087
- Bernhard E., Mullaney J. R., Daddi E., Ciesla L., Schreiber C., 2016, *MNRAS*
- Bieri R., Dubois Y., Silk J., Mamon G. A., Gaibler V., 2016, *MNRAS*, 455, 4166
- Bigiel F., Blitz L., 2012, *ApJ*, 756, 183
- Blanton M. R., Moustakas J., 2009, *ARA&A*, 47, 159
- Böker T., Falcón-Barroso J., Schinnerer E., Knapen J. H., Ryder S., 2008, *AJ*, 135, 479
- Bongiorno A., Merloni A., Brusa M., Magnelli B., Salvato M., Mignoli M., Zamorani G., Fiore F., et al. 2012, *MNRAS*, 427, 3103
- Booth C. M., Schaye J., 2010, *MNRAS*, 405, L1
- Carniani S., Marconi A., Maiolino R., Balmaverde B., Brusa M., Cano-Díaz M., Cicone C., Comastri A., et al. 2016, *ArXiv e-prints*
- Cicone C., Maiolino R., Sturm E., Graciá-Carpio J., Feruglio C., Neri R., Aalto S., Davies R., et al. 2014, *A&A*, 562, A21
- Croom S. M., Smith R. J., Boyle B. J., Shanks T., Miller L., Outram P. J., Loaring N. S., 2004, *MNRAS*, 349, 1397
- Faucher-Giguère C.-A., Quataert E., 2012, *MNRAS*, 425, 605
- Feruglio C., Maiolino R., Piconcelli E., Menci N., Aussel H., Lamastra A., Fiore F., 2010, *A&A*, 518, L155+
- Gaibler V., Khochfar S., Krause M., Silk J., 2012, *MNRAS*, 425, 438
- García-Burillo S., Combes F., Usero A., Aalto S., Colina L., Alonso-Herrero A., Hunt L. K., Arribas S., Costagliola F., Labiano A., Neri R., Pereira-Santaella M., Tacconi L. J., van der Werf P. P., 2015, *A&A*, 580, A35
- Hopkins P. F., Elvis M., 2010, *MNRAS*, 401, 7
- Kennicutt Jr. R. C., 1998, *ApJ*, 498, 541
- King A., 2003, *ApJL*, 596, L27
- King A., 2005, *ApJL*, 635, L121
- King A., Nixon C., 2015, *MNRAS*, 453, L46
- King A., Pounds K., 2015, *ARA&A*, 53, 115
- King A. R., 2010a, *MNRAS*, 408, L95
- King A. R., 2010b, *MNRAS*, 402, 1516
- King A. R., Pringle J. E., Hofmann J. A., 2008, *MNRAS*, 385, 1621
- King A. R., Zubovas K., Power C., 2011, *MNRAS*, 415, L6
- Knapen J. H., 2005, *A&A*, 429, 141
- Kormendy J., Kennicutt Jr. R. C., 2004, *ARA&A*, 42, 603
- Leroy A. K., Walter F., Brinks E., Bigiel F., de Blok W. J. G., Madore B., Thornley M. D., 2008, *AJ*, 136, 2782
- Merrett H. R., Merrifield M. R., Douglas N. G., Kuijken K., Romanowsky A. J., Napolitano N. R., Arnaboldi M., Capaccioli M., Freeman K. C., Gerhard O., Coccato L., Carter D., Evans N. W., Wilkinson M. I., Halliday C., Bridges T. J., 2006, *MNRAS*, 369, 120
- Momany Y., Zaggia S., Gilmore G., Piotto G., Carraro G., Bedin L. R., de Angeli F., 2006, *A&A*, 451, 515
- Mullaney J. R., Pannella M., Daddi E., Alexander D. M., Elbaz D., Hickox R. C., Bournaud F., Altieri B., et al. 2012, *MNRAS*, 419, 95
- Navarro J. F., Frenk C. S., White S. D. M., 1997, *ApJ*, 490, 493
- Nayakshin S., Power C., 2010, *MNRAS*, 402, 789
- Nayakshin S., Zubovas K., 2012, *MNRAS*, 427, 372
- Page M. J., Symeonidis M., Vieira J. D., Altieri B., Amblard A., Arumugam V., Aussel H., Babbedge T., et al. 2012, *Nature*, 485, 213
- Popping G., Somerville R. S., Trager S. C., 2014, *MNRAS*, 442, 2398
- Richards G. T., Strauss M. A., Fan X., Hall P. B., Jester

- S., Schneider D. P., Vanden Berk D. E., Stoughton C., et al. 2006, *AJ*, 131, 2766
- Riffel R. A., Storchi-Bergmann T., 2011a, *MNRAS*, 411, 469
- Riffel R. A., Storchi-Bergmann T., 2011b, *MNRAS*, 417, 2752
- Rupke D. S. N., Veilleux S., 2011, *ApJL*, 729, L27+
- Saintonge A., Kauffmann G., Kramer C., Tacconi L. J., Buchbender C., Catinella B., Fabello S., Graciá-Carpio J., et al. 2011, *MNRAS*, 415, 32
- Santini P., Rosario D. J., Shao L., Lutz D., Maiolino R., Alexander D. M., Altieri B., Andreani P., et al. 2012, *A&A*, 540, A109
- Sarzi M., Allard E. L., Knapen J. H., Mazzuca L. M., 2007, *MNRAS*, 380, 949
- Schawinski K., Koss M., Berney S., Sartori L. F., 2015, *MNRAS*, 451, 2517
- Shih H.-Y., Rupke D. S. N., 2010, *ApJ*, 724, 1430
- Silk J., 2005, *MNRAS*, 364, 1337
- Silk J., 2013, *ApJ*, 772, 112
- Silk J., Norman C., 2009, *ApJ*, 700, 262
- Soltan A., 1982, *MNRAS*, 200, 115
- Spence R. A. W., Zaurín J. R., Tadhunter C. N., Rose M., Cabrera-Lavers A., Spoon H., Muñoz-Tuñón C., 2016, *MNRAS*
- Sturm E., González-Alfonso E., Veilleux S., Fischer J., Graciá-Carpio J., Hailey-Dunsheath S., Contursi A., Poglitsch A., et al. 2011, *ApJL*, 733, L16+
- Tacchella S., Carollo C. M., Renzini A., Schreiber N. M. F., Lang P., Wuyts S., Cresci G., Dekel A., Genzel R., Lilly S. J., Mancini C., Newman S., Onodera M., Shapley A., Tacconi L., Woo J., Zamorani G., 2015, *Science*, 348, 314
- Tombesi F., Cappi M., Reeves J. N., Palumbo G. G. C., Yaqoob T., Braitto V., Dadina M., 2010a, *A&A*, 521, A57+
- Tombesi F., Meléndez M., Veilleux S., Reeves J. N., González-Alfonso E., Reynolds C. S., 2015, *Nature*, 519, 436
- Tombesi F., Sambruna R. M., Reeves J. N., Braitto V., Ballo L., Gofford J., Cappi M., Mushotzky R. F., 2010b, *ApJ*, 719, 700
- van der Kruit P. C., 1981, *A&A*, 99, 298
- Vollmer B., Nehlig F., Ibata R., 2016, *A&A*, 586, A98
- Wang J., Fu J., Aumer M., Kauffmann G., Józsa G. I. G., Serra P., Huang M.-l., Brinchmann J., van der Hulst T., Bigiel F., 2014, *MNRAS*, 441, 2159
- Xue Y. Q., Brandt W. N., Luo B., Rafferty D. A., Alexander D. M., Bauer F. E., Lehmer B. D., Schneider D. P., Silverman J. D., 2010, *ApJ*, 720, 368
- Zubovas K., 2015, *MNRAS*, 451, 3627
- Zubovas K., King A., 2012a, *ApJL*, 745, L34
- Zubovas K., King A. R., 2012b, *MNRAS*, 426, 2751
- Zubovas K., King A. R., 2014, *MNRAS*, 439, 400
- Zubovas K., Nayakshin S., King A., Wilkinson M., 2013, *MNRAS*, 433, 3079
- Zubovas K., Nayakshin S., Sazonov S., Sunyaev R., 2013, *MNRAS*, 431, 793
- Zubovas K., Sabulis K., Naujalis R., 2014, *MNRAS*, 442, 2837